

Modeling Leidenfrost Levitation of Soft Elastic Solids

Jack Binysh¹,¹ Indrajit Chakraborty²,² Mykyta V. Chubynsky,² Vicente Luis Díaz Melian,³ Scott R. Waitukaitis³,³ James E. Sprittles²,² and Anton Souslov^{1,*}

¹*Department of Physics, University of Bath, Claverton Down, Bath BA2 7AY, United Kingdom*

²*Mathematics Institute, University of Warwick, Coventry CV4 7AL, United Kingdom*

³*Institute of Science and Technology Austria (ISTA), Lab Building West, Am Campus 1, 3400 Klosterneuburg, Austria*



(Received 8 July 2022; revised 14 July 2023; accepted 5 September 2023; published 18 October 2023)

The elastic Leidenfrost effect occurs when a vaporizable soft solid is lowered onto a hot surface. Evaporative flow couples to elastic deformation, giving spontaneous bouncing or steady-state floating. The effect embodies an unexplored interplay between thermodynamics, elasticity, and lubrication: despite being observed, its basic theoretical description remains a challenge. Here, we provide a theory of elastic Leidenfrost floating. As weight increases, a rigid solid sits closer to the hot surface. By contrast, we discover an elasticity-dominated regime where the heavier the solid, the higher it floats. This geometry-governed behavior is reminiscent of the dynamics of large liquid Leidenfrost drops. We show that this elastic regime is characterized by Hertzian behavior of the solid's underbelly and derive how the float height scales with materials parameters. Introducing a dimensionless elastic Leidenfrost number, we capture the crossover between rigid and Hertzian behavior. Our results provide theoretical underpinning for recent experiments, and point to the design of novel soft machines.

DOI: [10.1103/PhysRevLett.131.168201](https://doi.org/10.1103/PhysRevLett.131.168201)

The elastic Leidenfrost effect represents a largely unexplored class of Leidenfrost physics, combining thermodynamics, flow, and elasticity [1–5]. In the liquid Leidenfrost effect, a fluid droplet hovers above a heated surface, cushioned by a gap layer of its own vapor. The basic physics of this scenario is extensively explored: capillarity and gravity determine the droplet's geometry and how high it floats above the hot surface [6–11]. These fundamental advances have enabled the discovery of new effects, such as self-propelled droplets [12] and controlled wetting [13], as well as the design of new applications, for example, heat exchangers [14,15].

The typical description of Leidenfrost physics combines flow and phase change, but neglects bulk 3D elastic deformation within the levitated object entirely [16–18]. Yet, the interplay between fluid flow and soft elastic response is known to yield a plethora of fluid-structure phenomena not possible in a purely rigid limit [19–33]. So it proves in the elastic Leidenfrost effect: when the levitated object is soft and elastic, striking effects result. For example, a water-saturated hydrogel lowered onto a hot surface either bounces spontaneously [1,2] or floats on its own vapor layer [3]. Figure 1(a) shows an example of floating behavior

for a sphere of radius 7 mm. These effects may appear superficially similar to the phenomenology of liquids [9,34], but they arise from a distinct interplay between the vapor phase and the condensed phase. In the levitation of Leidenfrost liquids, excess pressure in the vapor layer competes with surface tension [9–11,34]. By contrast, in a soft elastic solid [Fig. 1(a)] the characteristic feature of both bouncing and floating is that the excess pressure in the vapor layer (of order kilopascals) competes with bulk 3D elastic stress [1].

Soft materials thus invite us to reexamine the fundamentals of Leidenfrost physics when combined with large solid-body deformations. However, to fully realize the scope of the elastic Leidenfrost effect, both at a fundamental level and for the potential design of soft devices, a theoretical description of the basic mechanism is required. Despite experimental observation, this description remains a challenge. In particular, there is currently no theory which explains how three-dimensional elasticity determines either the levitation height of the soft solid, or its shape in the floating regime.

In this Letter, we overcome this challenge by marrying thermodynamic phase change with the lubrication theory of soft elastic objects [19–26,33], to formulate the first description of elastic Leidenfrost floating. By varying a single dimensionless parameter, we discover a transition from rigid behavior to an elasticity-dominated regime described by Hertzian contact mechanics. Using asymptotic analysis and finite element simulations, we quantify this Hertzian limit via scaling laws for the gap height with

Published by the American Physical Society under the terms of the [Creative Commons Attribution 4.0 International license](https://creativecommons.org/licenses/by/4.0/). Further distribution of this work must maintain attribution to the author(s) and the published article's title, journal citation, and DOI.

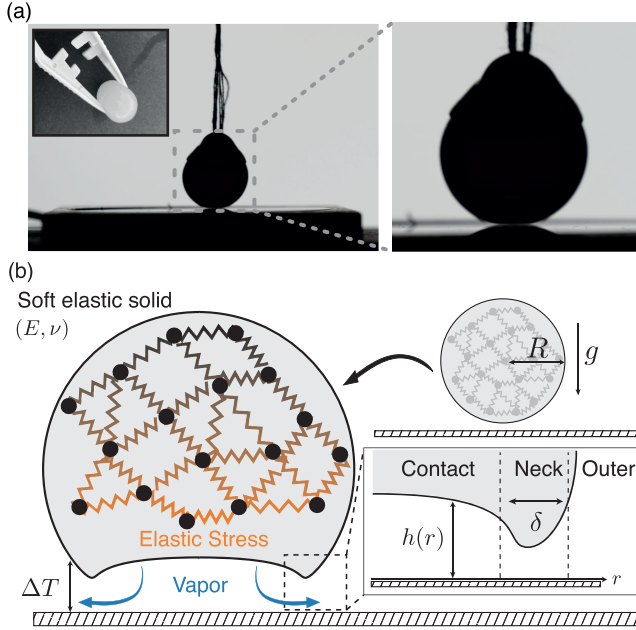


FIG. 1. Leidenfrost levitation of elastic solids enabled by soft lubrication. (a) A soft elastic hydrogel sphere of radius $R = 7$ mm hovers above a hot surface ($\Delta T = 115^\circ\text{C}$). The inset shows hydrogel in daylight. (b) Evaporative flux elastically deforms the soft solid. Competition between vapor pressure and elastic stress sets the shape of the solid's underbelly and the gap height. Inset: we predict distinct height scaling laws in a contact region under the soft solid, an outer region, and a narrow neck region of width δ .

sphere radius and elastic modulus. Our asymptotic theory reveals the existence of two distinct scalings of the height: the first in a contact region well underneath the solid, and the second in an ever-narrowing neck region [see Fig. 1(b)]. The development of a neck is also observed for large liquid Leidenfrost drops [8,10,11] and our results invite the question of how liquid Leidenfrost phenomenology intersects with that of soft Leidenfrost solids. More broadly, our results demonstrate how to tailor float height via materials properties, and offer a solid theoretical basis for exploring more complex elastic Leidenfrost phenomena. This theory lays the groundwork for combining elasticity, phase change, and flow to design novel soft machines.

Our first main result is that elastic response yields a new class of scaling laws for the gap height h of floating Leidenfrost objects. This elastic scaling law is distinct from both the liquid and rigid solid cases. A stiff vaporizable sphere (or small liquid drop [7]) of radius R , density ρ_s , and weight $F = (4\pi/3)\rho_s g R^3$ floats at a height $h \sim F^{-1/2}R$ above a heated surface. Taking the load to be proportional to the volume $F \sim R^3$, we have $h \sim R^{-1/2}$: intuitively, balancing an increasing radius R (i.e., an increasing weight) requires more vapor flux, and so a stiff solid must sit closer to the heated surface. By contrast, we find that a vaporizable

elastic sphere of Young's modulus E and Poisson ratio ν (Fig. 1) has a gap height that scales as

$$h \sim \Pi_0^{1/4} E^{-1/3} R^{1/3} F^{1/12}. \quad (1)$$

In Eq. (1), Π_0 models the thermal and viscous properties of the vapor layer, and is defined below. Again taking $F \sim R^3$ we find the height scaling $h \sim R^{7/12}$: counterintuitively, the heavier the soft solid, the higher it floats.

To derive Eq. (1) we now formulate a theory of phase-change induced lubrication coupled to elastic deformation of the solid. Figure 1(b) shows a schematic of the soft solid floating above a hot surface. The heated surface is held at a temperature difference ΔT above the vaporization threshold of the solid, causing the solid's underbelly to evaporate and open a thin vapor gap. To describe vapor flow, we note that the gap height is significantly smaller than the lateral scale of the underbelly. We will verify that this observation is indeed self-consistent below. We use the lubrication approximation of the Navier-Stokes equations [10,22], which neglects the vertical component of flow. In this approximation, the (axisymmetric) height profile $h(r)$ in Fig. 1(b) and the pressure in the vapor layer $P(r)$ are related through

$$\frac{1}{r} \frac{d}{dr} \left(r \frac{\rho h(r)^3}{12\eta} \frac{dP(r)}{dr} \right) = -\frac{\kappa \Delta T}{Lh(r)}. \quad (2)$$

Equation (2) expresses continuity: the pressure gradient under the solid establishes a Poiseuille flow with mass flux $\sim (\rho/\eta)h^3 \nabla P(r)$, where η and ρ are the viscosity and density of the vapor. This flux is balanced by a Leidenfrost source term $-\kappa \Delta T/Lh(r)$, describing conduction-dominated evaporation from the solid's underbelly [10]. Here, κ is the vapor thermal conductivity and L is the latent heat of vaporization. The materials parameters in Eq. (2) define a typical force scale within the vapor layer, $\Pi_0 \equiv \kappa \Delta T \eta / L \rho$ [17] [see Eq. (1)]. Nondimensionalized by the elastogravitational force scale $E^3 / (\rho g)^2$, Π_0 represents the elastic analog of the evaporation number found in liquid Leidenfrost physics [10,11]. Using Π_0 , Eq. (2) can be rearranged so that the source term is simply $-\Pi_0/h(r)$.

For a steady gap height, integrated vapor pressure must balance the total weight F of the solid. If the pressure P acts over a lateral length scale l characteristic of the solid's underbelly, we have the scaling $F \sim Pl^2$. A scaling analysis of the lubrication equation Eq. (2) relates P , l , and gap height h as $P \sim \Pi_0 l^2 / h^4$. Using this pressure relation in the total force balance gives

$$F \sim \Pi_0 \left(\frac{l}{h} \right)^4. \quad (3)$$

For a given load F , Eq. (3) specifies h in terms of an unknown lateral scale l . The crucial question is, then, what

is the correct choice of l ? We postulate that there are two choices of l , giving two possible gap height scaling laws. The first choice is for a completely rigid sphere, neglecting elasticity: $l_S = \sqrt{hR}$ [23]. Using this choice in Eq. (3) recovers the height scaling for rigid spheres, $h \sim \sqrt{\Pi_0/FR}$. This scaling applies whenever geometric deformation can be neglected [7,11].

Scaling laws unique to elastic Leidenfrost floating result from a different choice of lateral length scale l , arising from linear elasticity theory and Hertzian contact mechanics [35–37]: we describe this regime as one of Hertzian scaling. When an elastic sphere of Young’s modulus E is placed in direct contact with a hard surface, a circular indentation results, with radius $l_H \sim (FR/E)^{1/3} \sim R^{4/3}$. We hypothesize that the underbelly of an elastic Leidenfrost solid asymptotically adopts this lateral scale. The total vapor thrust then scales as the ratio $(l_H/h)^4$, but the total load scales as the volume R^3 , resulting in a float height given by $h \sim l_H/R^{3/4} \sim R^{7/12}$. Note that $h/l_H \sim R^{-3/4}$, and so the lubrication approximation improves as we go further into the Hertzian limit.

The full scaling with all materials parameters is given in Eq. (1). Intuitively, as the sphere radius increases, elastic deformation of the solid’s underbelly gives a rapidly increasing contact area over which evaporative thrust is generated. This increasing thrust outcompetes the increasing weight, leading to the counterintuitive increase of gap height with radius R . In the discussion, we compare this behavior to that of large liquid Leidenfrost drops, which also exhibit a regime of increasing gap height with lateral extent [6,8,10,11].

We have described two distinct scaling regimes for the gap height of elastic Leidenfrost solids: a stiff regime characterized by the lateral length scale l_S , and a Hertzian regime characterized by l_H . Our second main result is to show that the crossover between these regimes is characterized by a single dimensionless elastic Leidenfrost number λ , defined as

$$\lambda \equiv \frac{2\pi}{3} \left[\frac{l_S}{l_H} \right]^4 = \frac{2\pi}{3} \left[\frac{4E}{3(1-\nu^2)} \right]^{4/3} \Pi_0 F^{-7/3} R^{8/3}. \quad (4)$$

Intuitively, λ compares the length scales over which vapor pressure causes elastic deformation, as shown by the first equality in Eq. (4). The second equality provides an expression in terms of materials parameters. When $\lambda \rightarrow \infty$, $l_S \gg l_H$ and vapor pressure is too small to cause appreciable elastic deformation. By contrast, when $\lambda \rightarrow 0$, $l_S \ll l_H$ and Hertzian elasticity dominates. A crossover between the rigid and Hertzian regimes is expected at $\lambda \sim 1$. In Supplemental Material (SM) [38], we show that nondimensionalizing the combined equations of linear elasticity and the lubrication equation [i.e., Eq. (2)] yields λ as the single dimensionless number governing the floating regime.

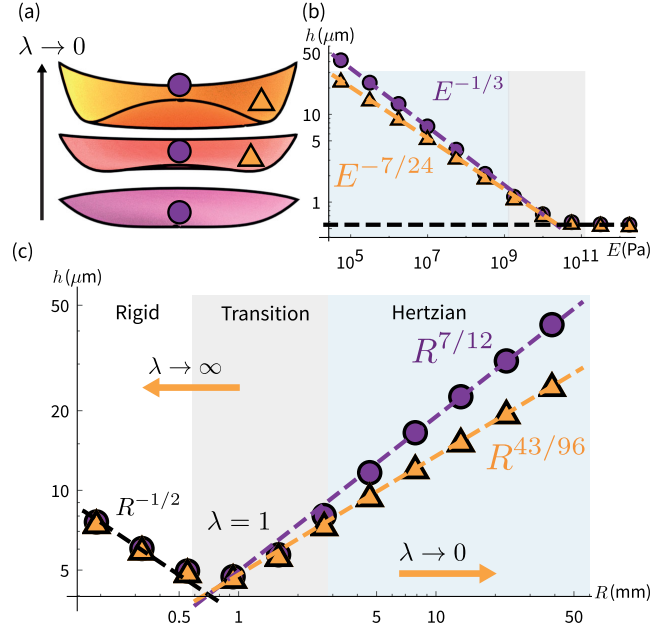


FIG. 2. Gap height scaling laws. (a) Profiles of the solid’s underbelly in the Hertzian limit $\lambda \rightarrow 0$ show the development of a neck region (orange triangle), with height scaling law distinct from the contact region (purple circle). (b),(c) Finite element simulations (markers) verify our analytically predicted gap height scaling laws (lines) for the contact ($h \sim E^{-1/3} R^{7/12}$) and neck ($h \sim E^{-7/24} R^{43/96}$) regions. Black lines show analytic predictions for a rigid sphere. We find three regimes: rigid ($\lambda \rightarrow \infty$), transition ($\lambda \sim 1$), and Hertzian ($\lambda \rightarrow 0$). In (b), $R = 40$ mm. In (c), $E = 50$ kPa. Remaining parameters as in [3].

We have predicted that the dimensionless parameter λ mediates the crossover between rigid behavior and our scaling law, Eq. (1). We now test these predictions. To do so, we numerically solve for a series of profiles for the gap height $h(r)$ and for the pressure $P(r)$, across a range of sphere radii and Young’s moduli. We implement a hybrid finite element method in COMSOL multiphysics, in which the equations of linear elasticity are solved throughout the 3D solid. This elastic solver is coupled to a numerical solution of the lubrication equation Eq. (2) via COMSOL’s standard Coefficient Form Boundary PDE option. Our finite element approach, described further in SM [38], was used in Refs. [42,43] to study droplet impact and the liquid Leidenfrost effect. This method allows us to probe the limits of validity for our theory by bypassing the assumptions made in Hertzian contact theory, i.e., the use of a half-space elastic solution for a curved boundary and a parabolic approximation to the solid’s underbelly.

In Fig. 2, we show the gap height in the contact region, $h(r=0)$, against radius R and modulus E . Parameters not varied are fixed to natural experimental values for the hydrogel spheres used in, for example, Ref. [3]. We find a clear crossover between two distinct regimes of behavior occurring at $\lambda \sim 1$, with agreement between our predicted

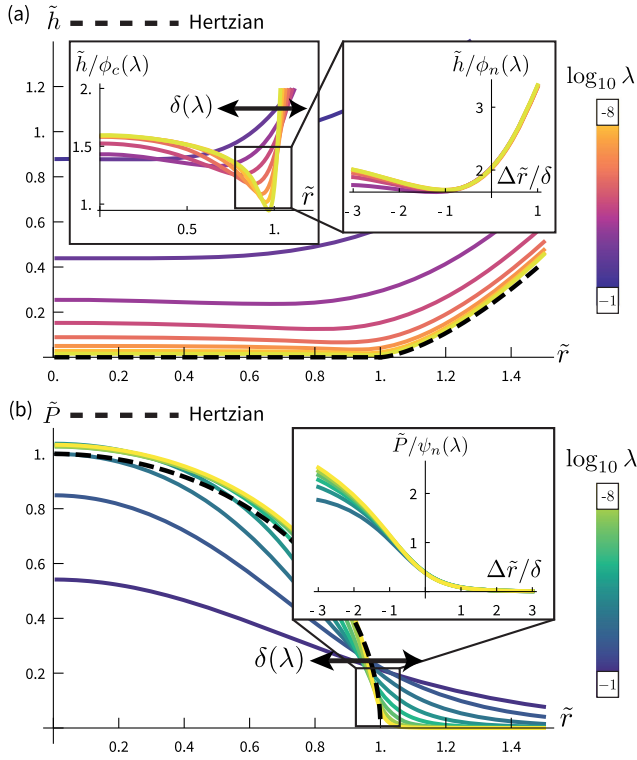


FIG. 3. Collapsing to the Hertzian limit. Nondimensionalized (a) height \tilde{h} and (b) pressure \tilde{P} profiles from finite element simulation. Both approach the Hertzian solutions (black dashed lines) as $\lambda \rightarrow 0$. Deviations are confined to the neck region $\delta(\lambda)$. Insets: our height scaling law in the contact region, $\phi_c(\lambda) = \lambda^{1/4}$, breaks down in the neck [(a), left]. Instead, our asymptotic theory predicts that profiles collapse in the neck when radius $\Delta\tilde{r} \equiv \tilde{r} - 1$ is rescaled by $\delta(\lambda) = \lambda^{3/16}$, height by $\phi_n(\lambda) = \lambda^{9/32}$ [(a), right] and pressure by $\psi_n(\lambda) = \lambda^{3/32}$ [(b) right].

scaling laws, Eq. (1), and those found in simulation. However, our numerical results also reveal a neck region at the edge of contact [Fig. 2(a)], which develops as the solid transitions into the Hertzian regime. The height of this neck follows a distinct scaling law, not captured by the analysis above.

To study this neck region further, in Fig. 3 we plot the full height [Fig. 3(a)] and pressure [Fig. 3(b)] profiles under the soft solid, nondimensionalized by Hertzian scales: $\tilde{r} = r/l_H$, $\tilde{h} = hR/l_H^2$, $\tilde{P} = (2\pi l_H^2/3F)P$. As $\lambda \rightarrow 0$ both height and pressure profiles approach their Hertzian limits, $\tilde{h}(\tilde{r}) = (\tilde{r} - 1)^{3/2}$ for $\tilde{r} \gtrsim 1$, and $\tilde{P}(\tilde{r}) = \sqrt{1 - \tilde{r}^2}$ for $\tilde{r} < 1$ [36], except in a boundary layer of width $\delta(\lambda)$ located at $\tilde{r} = 1$. The discrepancy in the height data becomes clearer when we rescale \tilde{h} by the contact scaling law Eq. (1). We show in SM [38] that Eq. (1) corresponds to the dimensionless scaling law $\tilde{h}(\tilde{r} = 0) \sim \phi_c(\lambda)$, where $\phi_c(\lambda) = \lambda^{1/4}$. As shown in the left inset of Fig. 3(a), this law collapses data in the contact region, but fails in the neck $\delta(\lambda)$. The reason is that the Hertzian dry contact solutions are singular at $\tilde{r} = 1$. This singularity implies a breakdown of Hertz theory over

the width $\delta(\lambda)$, because the height and pressure profiles in our lubrication problem must remain smooth everywhere. In this region, the height scaling from Eq. (1) does not apply because the relevant lateral length scale is no longer the Hertzian length scale l_H .

To capture the anomalous scaling of the height in the neck region and the width $\delta(\lambda)$, we take inspiration from the numerical collapse of Fig. 3. The key observation is that in the contact region under the solid ($\tilde{r} \ll 1$), the pressure is given by the Hertzian solution at leading order in the parameter λ [Fig. 3(b)]. By the same logic, when $\tilde{r} \gg 1$, the height is asymptotically Hertzian [Fig. 3(a)]. Using the lubrication equation Eq. (2), we construct the corresponding height and pressure solutions in each region. These solutions patch together over the neck region, shown schematically in the inset of Fig. 1(b). In the neck, both pressure and height vanish as some unknown power of λ ; we denote the height scaling as $\phi_n(\lambda)$ and the pressure scaling as $\psi_n(\lambda)$. The patching conditions, derived in SM [38], determine $\delta(\lambda)$, $\phi_n(\lambda)$, and $\psi_n(\lambda)$ to give a complete set of scaling laws:

$$\begin{aligned} \delta(\lambda) &= \lambda^{3/16}, & \phi_c(\lambda) &= \lambda^{1/4}, \\ \psi_n(\lambda) &= \lambda^{3/32}, & \phi_n(\lambda) &= \lambda^{9/32}. \end{aligned} \quad (5)$$

In the insets of Fig. 3, we show that the scalings Eq. (5) now collapse our simulation data in the neck region as well as the contact region. Our asymptotic theory gives a new prediction: redimensionalized, the relation $\phi_n(\lambda) = \lambda^{9/32}$ yields the anomalous neck height scaling

$$h \sim \Pi_0^{9/32} E^{-7/24} F^{1/96} R^{5/12}. \quad (6)$$

Again taking the load to go as the volume, $F \sim R^3$, we find the neck height scaling $h \sim R^{43/96}$. In Fig. 2, we show that these revised scalings with radius R and modulus E agree well with simulations. Taken together, the scalings Eqs. (1) and (6) provide a complete picture of elastic Leidenfrost floating, with the agreement between the asymptotic result Eq. (6) and our simulations also serving as a rigorous cross-check on our theory.

Our fundamental description of elastic Leidenfrost floating provides the theoretical groundwork for interpreting recent studies [1,3], and establishes principles for experimental investigation of this new class of Leidenfrost phenomena. Using hydrogel spheres of radius $R = 7$ mm and modulus $E = 50$ kPa, Ref. [3] places an upper bound on the gap height in the floating regime as $h < (25 \pm 10)$ μm . Our theory predicts a contact height of $h = 15$ μm and a neck height of $h = 12$ μm , and finds $\lambda \sim 10^{-5}$, placing the experiments of Ref. [3] in the regime of Hertzian scaling governed by Eq. (1). Gap heights of ~ 15 μm are measurable via interferometric imaging, although inferring absolute height data in this range requires techniques beyond

white-light interferometry: in SM we describe the experimental methodology necessary to probe our theoretical scaling laws.

Before chimneying, large liquid Leidenfrost drops also exhibit a regime of increasing float height with lateral extent, and the development of a neck [6,8,10,11]. The mechanism behind this regime, both in liquids and the soft elastic solids considered here, is geometric change occurring on the underbelly of the levitated object. However, scaling relations differ between the liquid and soft solid cases [10]. For example, we find neck height scaling $h \sim R^{43/96}$, whereas in Ref. [11] the neck height appears to plateau at a constant value. Our Letter invites the question of how much of the rich phenomenology of liquids finds an elastic counterpart [44,45].

More broadly, our Letter points toward combining Leidenfrost-type physics and soft elasticity beyond the setup of Fig. 1(a). We envision tailoring the floating configuration of an object by combining phase-change induced forces with those from motion [23,25], and by tuning initial geometry: in SM [38], we show that an elastic cylinder in the Hertzian regime has a contact height scaling $h \sim R^{5/8}$, distinct from the spherical case. Such shape control is not possible for liquid droplets.

The supporting data for this Letter are openly available from Zenodo under an MIT license Ref. [46].

We are grateful to Dominic Vella, Jens Eggers, John Kolinski, Joshua Dijkstra, and Daniel Bonn for insightful discussions. J. B. and A. S. acknowledge the support of the Engineering and Physical Sciences Research Council (EPSRC) through New Investigator Award No. EP/T000961/1. A. S. acknowledges the support of Royal Society under Grant No. RGS/R2/202135. J. E. S. acknowledges EPSRC Grants No. EP/N016602/1, EP/S022848/1, EP/S029966/1, and EP/P031684/1.

* A.Souslov@bath.ac.uk

[1] S. R. Waitukaitis, A. Zúñiga-Wilk, A. Souslov, C. Coullais, and M. van Hecke, *Nat. Phys.* **13**, 1095 (2017).
 [2] J. T. Pham, M. Paven, S. Wooh, T. Kajiyama, H.-J. Butt, and D. Vollmer, *Nat. Commun.* **8**, 905 (2017).
 [3] S. Waitukaitis, K. Harth, and M. van Hecke, *Phys. Rev. Lett.* **121**, 048001 (2018).
 [4] H. K. Khattak, P. Bianucci, and A. D. Slepko, *Proc. Natl. Acad. Sci. U.S.A.* **116**, 4000 (2019).
 [5] H. K. Khattak, S. R. Waitukaitis, and A. D. Slepko, *Soft Matter* **15**, 5804 (2019).
 [6] A.-L. Biance, C. Clanet, and D. Quéré, *Phys. Fluids* **15**, 1632 (2003).
 [7] F. Celestini, T. Frisch, and Y. Pomeau, *Phys. Rev. Lett.* **109**, 034501 (2012).
 [8] J. C. Burton, A. L. Sharpe, R. C. A. van der Veen, A. Franco, and S. R. Nagel, *Phys. Rev. Lett.* **109**, 074301 (2012).
 [9] D. Quéré, *Annu. Rev. Fluid Mech.* **45**, 197 (2013).

[10] B. Sobac, A. Rednikov, S. Dorbolo, and P. Colinet, *Phys. Rev. E* **90**, 053011 (2014).
 [11] B. Sobac, A. Rednikov, S. Dorbolo, and P. Colinet, *Phys. Rev. E* **103**, 039901(E) (2021).
 [12] H. Linke, B. J. Alemán, L. D. Melling, M. J. Taormina, M. J. Francis, C. C. Dow-Hygelund, V. Narayanan, R. P. Taylor, and A. Stout, *Phys. Rev. Lett.* **96**, 154502 (2006).
 [13] T. Tran, H. J. J. Staat, A. Prosperetti, C. Sun, and D. Lohse, *Phys. Rev. Lett.* **108**, 036101 (2012).
 [14] H. Van Dam, *Rep. Prog. Phys.* **55**, 2025 (1992).
 [15] I. U. Vakarelski, N. A. Patankar, J. O. Marston, D. Y. Chan, and S. T. Thoroddsen, *Nature (London)* **489**, 274 (2012).
 [16] G. Dupeux, M. Le Merrer, G. Lagubeau, C. Clanet, S. Hardt, and D. Quéré, *Europhys. Lett.* **96**, 58001 (2011).
 [17] G. Dupeux, T. Baier, V. Bacot, S. Hardt, C. Clanet, and D. Quéré, *Phys. Fluids* **25**, 051704 (2013).
 [18] G. G. Wells, R. Ledesma-Aguilar, G. McHale, and K. Sefiane, *Nat. Commun.* **6**, 1 (2015).
 [19] C. J. Hooke and J. P. O'Donoghue, *J. Mech. Eng. Sci.* **14**, 34 (1972).
 [20] J. Archard, *J. Mech. Eng. Sci.* **10**, 165 (1968).
 [21] K. Johnson, *J. Mech. Eng. Sci.* **12**, 9 (1970).
 [22] B. J. Hamrock, S. R. Schmid, and B. O. Jacobson, *Fundamentals of Fluid Film Lubrication* (Marcel Dekker, New York City, 2004).
 [23] J. M. Skotheim and L. Mahadevan, *Phys. Rev. Lett.* **92**, 245509 (2004).
 [24] J. H. Snoeijer, J. Eggers, and C. H. Vennert, *Phys. Fluids* **25**, 101705 (2013).
 [25] M. H. Essink, A. Pandey, S. Karpitschka, C. H. Vennert, and J. H. Snoeijer, *J. Fluid Mech.* **915**, A49 (2021).
 [26] J. A. Greenwood, *Lubricants* **8**, 51 (2020).
 [27] C. Duprat and H. A. Shore, *Fluid-Structure Interactions in Low-Reynolds-Number Flows* (Royal Society of Chemistry, Cambridge, UK, 2015).
 [28] T. Gervais, J. El-Ali, A. Günther, and K. F. Jensen, *Lab Chip* **6**, 500 (2006).
 [29] I. C. Christov, V. Cognet, T. C. Shidhore, and H. A. Stone, *J. Fluid Mech.* **841**, 267 (2018).
 [30] S. Leroy, A. Steinberger, C. Cottin-Bizonne, F. Restagno, L. Léger, and E. Charlaix, *Phys. Rev. Lett.* **108**, 264501 (2012).
 [31] V. Bertin, Y. Amarouchene, E. Raphael, and T. Salez, *J. Fluid Mech.* **933**, A23 (2022).
 [32] A. Kargar-Estahbanati and B. Rallabandi, *Phys. Rev. Fluids* **6**, 034003 (2021).
 [33] B. J. Hamrock and D. Dowson, *J. Lubr. Technol.* **98**, 223 (1976).
 [34] G. Graeber, K. Regulagadda, P. Hodel, C. Küttel, D. Landolf, T. M. Schutzius, and D. Poulikakos, *Nat. Commun.* **12**, 1727 (2021).
 [35] L. Landau and E. Lifshitz, *Theory of Elasticity* (Elsevier Science, New York, 1986).
 [36] K. L. Johnson, *Contact Mechanics* (Cambridge University Press, Cambridge, England, 1985).
 [37] E. J. Bissett, *Proc. R. Soc. A* **424**, 393 (1989).
 [38] See Supplemental Material at <http://link.aps.org/supplemental/10.1103/PhysRevLett.131.168201>, which includes Refs. [39–41] for the asymptotic analysis leading to

- the scaling laws Eq. (5), a description of our finite element simulation method and a detailed discussion of the interferometric methodology needed to test our predictions.
- [39] K. F. Riley, M. P. Hobson, and S. J. Bence, *Mathematical Methods for Physics and Engineering* (American Association of Physics Teachers, Cambridge, UK, 1999).
- [40] M. Abramowitz and I. A. Stegun, *Handbook of Mathematical Functions with Formulas, Graphs, and Mathematical Tables* (US Government printing office, 1964), Vol. 55.
- [41] R. C. A. vanderVeen, T. Tran, D. Lohse, and C. Sun, *Phys. Rev. E* **85**, 026315 (2012).
- [42] M. V. Chubynsky, K. I. Belousov, D. A. Lockerby, and J. E. Sprittles, *Phys. Rev. Lett.* **124**, 084501 (2020).
- [43] I. Chakraborty, M. V. Chubynsky, and J. E. Sprittles, *J. Fluid Mech.* **936**, A12 (2022).
- [44] A. Bouillant, T. Mouterde, P. Bourriane, A. Lagarde, C. Clanet, and D. Quéré, *Nat. Phys.* **14**, 1188 (2018).
- [45] A. Bouillant, C. Cohen, C. Clanet, and D. Quéré, *Proc. Natl. Acad. Sci. U.S.A.* **118**, e2021691118 (2021).
- [46] J. Binysh, I. Chakraborty, M. V. Chubynsky, V. L. Diaz Melian, S. R. Waitukaitis, J. E. Sprittles, and A. Souslov, Modelling Leidenfrost Levitation of Soft Elastic Solids, v1.0.1, Zenodo, [10.5281/zenodo.8329176](https://doi.org/10.5281/zenodo.8329176) (2023).